Singlet exciton diffusion length in organic light-emitting diodes

Simone Hofmann,[*] Thomas C. Rosenow,[†] Malte C. Gather, Björn Lüssem, and Karl Leo[‡]
Institut für Angewandte Photophysik, Technische Universtät Dresden, George-Bähr-Strasse 1, 01062 Dresden, Germany
(Received 29 February 2012; published 20 June 2012)

We present a simple and accurate method to determine the singlet diffusion length in an operating organic light-emitting device (OLED). By using electrical rather than optical excitation, the method ensures that excitons are formed in a tightly confined generation zone, from which they can diffuse towards a quenching material. For a series of devices with varying distance between generation and quenching region, different emission intensities are found, and the experimentally obtained emission spectra of these devices can be used to determine the singlet diffusion length in the emissive layer of the device. By carefully choosing OLED layer materials and thicknesses, we can ensure well-defined quenching and blocking boundary conditions and exclude cavity effects as well as emission from the quenching material. An analytical model is developed to analyze the emission intensity found experimentally. We show that disregarding the fact that the generation zone has a nonzero width leads to an overestimation of the diffusion length. Furthermore, the current, i.e., the excitation density dependency of the singlet diffusion length, is investigated. At low current density (0.15 mA/cm^2), a singlet diffusion length of 4.6 $\pm$ 0.5 nm is obtained in N,N′-di-1-naphthalenyl-N,N′-diphenyl-[1,1′:4′,1″:4″,1‴-quaterphenyl]-4,4‴-diamine (4P-NPD). The singlet diffusion length decreases to 4.0 $\pm$ 0.5 nm at 154.08 mA/cm^2.

DOI: 10.1103/PhysRevB.85.245209 PACS number(s): 71.35.Cc, 81.05.Fb, 85.60.−q

I. INTRODUCTION

Organic thin film devices, including organic light-emitting diodes (OLEDs) and solar cells, gained much interest in recent years due to their high potential in various applications. In particular, efficiencies reported for OLEDs are already comparable to conventional high efficiency light sources.[1,2] The understanding and controlling of excitonic processes in OLEDs is important to achieve high efficiencies. For example, in white OLEDs comprising a fluorescent blue emitter and green/red phosphorescent emitters, the singlet excitons might migrate to the phosphorescent emitter and are transferred to an energetically deeper lying singlet level, which results in an undesired lowering of the blue emission.[3,4] Hence, an important parameter for device understanding and design, in particular of white OLEDs, is the singlet diffusion length.[5,6]

Early investigations on exciton interaction and diffusion have been performed on anthracene crystals in the 1960's and 70's.[7–9] For example, Avakian *et al.*[7] excited crystals with a laser through a grating to generate narrow parallel sections on the sample. The dependence of the emitted blue intensity from the sample on the ruling linewidth has been used to calculate the diffusion length.

Nowadays, common methods to determine the exciton diffusion length are based on photo-current measurements[10–14] and time- or spectral-resolved photoluminescence quenching.[15–23] However, these techniques have certain disadvantages resulting in a wide spread of the reported values of the diffusion length, even for well known materials like 4,4′-bis(carazol-9-yl1,1′-biphenyl (CBP)[14,23] or 3,4,9,10-perylenetetracarboxylic dianhydride (PTCDA).[22,23] Additionally, optical excitation leads to a broad generation zone of the excitons, the profile of which is usually an unknown parameter, complicating the analysis. Also, when using an additional quenching layer, optical interference effects and energy transfer to the quencher have to be taken into account.[24]

In contrast, electrical generation of excitons in an adequate OLED structure can lead to a thin and well-controllable generation zone adjacent to one of the blocking layers. Furthermore, the extracted value for the diffusion length inside a working device is of higher interest for device optimization, since it might differ from the one obtained by optical excitation, where, e.g., quenching with polarons is not present.

To determine the diffusion length of the triplet excitons the harvesting approach can be used.[25–28] The usually lost triplets of a fluorescent emitter are diffusing through a spacer layer towards a phosphorescent dopant, are transferred to the deeper lying triplet level of the dopant, and emit light. By varying the thickness of the spacer and the measured emission of the dopant, the triplet diffusion length is calculated. The weak microcavity effects can be overcome by an appropriate adjustment of the transport layer thickness, which keeps the emission zone at a constant position inside the device. One problem here is that the phosphorescent emitter also shows direct recombination, resulting in additional emission, which has to be considered in the analysis. In particular, it is important to take into account that the generation zone has a non-negligible width. For singlets this technique has been hardly used so far, and in addition the width of the generation zone was not considered in previous studies.[29,30]

The investigation of the diffusion length of excitons in operating devices goes side by side with the examination of the emission profile. Although the main loss channels in OLEDs are known, the emission profile, which is a key parameter for exact device modeling, has been hardly investigated.[31,32] In 2009, Gather *et al.*[33] extracted the profile of the emission zone for polymer OLEDs using a simulation of the emitted spectrum. A method claiming nanometer spatial resolution was introduced by Mensfoord *et al.* in 2010.[34] However, this technique requires the experimental effort of measuring angle and polarization resolved emission spectra. Furthermore, the emission profile in polymer OLEDs is broader than in small-molecule devices. The thin (10–20 nm) emission layer (EML) in typical small-molecule OLEDs makes it far more difficult to extract this property. Tang *et al.*[29] and later Choukri *et al.*[30]

found monoexponential emission profiles in small-molecule OLEDs by introducing a thin quenching layer (QL) at different distances from the generation zone.

In this paper, we report a simple and direct measurement method to simultaneously obtain the emission profile as well as the singlet diffusion length in N,N′-di-1-naphthalenyl-N,N′-diphenyl-[1,1′:4′,1″:4″,1‴-quaterphenyl]-4,4‴-diamine (4P-NPD). Using a carefully designed OLED structure, we achieve a narrow exciton generation zone, can neglect optical microcavity effects, and have no additional emission from the quenching material. The method is based on measuring the reduction of the emission from singlet excitons after inserting a quenching material at different distances from the generation zone. We apply an analytical model to extract the singlet diffusion length, which shows that disregarding the fact that the generation zone has a nonzero width leads to an overestimation of the diffusion length.

In the experimental section (Sec. II) we describe the sample preparation and materials, the measurement instruments, and the working principle of the device. The theory part (Sec. III) contains a solution of the diffusion equation and the function used to fit the experimental data. In Sec. IV we investigate the width of the generation zone and the dependence of the singlet diffusion length on the applied current. Finally, we summarize the results and draw conclusions in the last section (Sec. V).

II. EXPERIMENTAL

A. Sample preparation and materials

All organic materials are commercially purchased and further purified by vacuum gradient sublimation. Devices are processed on commercial, precleaned, prestructured indium tin oxide (ITO) coated glass substrates. The organic layers and the aluminum (Al) cathode are deposited by thermal evaporation in a UHV chamber (Kurt J. Lesker Co.) at a base pressure of about 10^{-7} mbar without breaking the vacuum. Evaporation rates of 2 Å/s, 0.8 to 1.0 Å/s, and 0.2 to 0.3 Å/s are used for Al, the transport layers, and the remaining organic layers, respectively. The thickness of all layers is measured *in situ* via quartz crystals. Doping is achieved by coevaporation.

After processing, the OLEDs are immediately encapsulated in nitrogen atmosphere using glass lids which include a getter material. The active area of all devices is 6.49 mm^2. Using mask systems, it is possible to wedge certain properties including thicknesses and concentrations from sample to sample. Hence, a total of 16 different device structures could be fabricated on a single substrate eliminating possible run-to-run variability.

The monochrome blue OLEDs employ blocking and doped charge transport layers.[35,36] We use N,N,N′,N′-tetrakis (4-methoxyphenyl)-benzidine (MeO-TPD) doped with 2 wt% 2,2′- (perfluoronaphthalene-2,6-diylidene)dimalononitrile (F6-TCNNQ) as *p*-type hole injection and transport layer (HTL). The *n*-type electron injection and transport layer (ETL) is 4,7-diphenyl-1,10-phenanthroline (BPhen) doped with cesium (Cs). Both transport layers exhibit a conductivity of 10^{-5} S/cm. 10 nm of 2,2′,7,7′-tetrakis-(N,N-diphenylamino)-9,9′-spirobifluoren (Spiro-TAD) and 10 nm of BPhen are implemented as electron and hole blocking layer (HBL), respectively, to confine charge carriers and excitons in the emission layer. As blue emission layer, we use the fluorescent 4P-NPD.[3,25,37] To quench the fluorescence 5 wt% of tris(2-phenylpyridine) iridium(III) [$Ir(ppy)_3$] is doped into 4P-NPD. The thickness of the different layers is summarized in Fig. 2(a). Single layers of 10 nm 4P-NPD and $Ir(ppy)_3$ doped into 4, 4′, 4″-tris(carbazol-9-yl)-triphenylamine (TCTA) with 10 wt% are prepared on cleaned quartz substrates in a multichamber evaporation tool (BesTec) at a base pressure of 10^{-7} mbar.

B. Measurement instruments

All OLED characterizations are done in air and at ambient temperature. Current-voltage (IV) measurements are performed with a Keithley SMU2400 source-measure unit. The spectral radiance in forward direction is recorded by a calibrated Instrument Systems GmbH CAS140 spectrometer. As the singlet diffusion length will be derived from thickness dependent measurements, the density of the material under investigation is very important. For this, the density of 4P-NPD is determined by profilometer and x-ray reflection measurements to 1.1 g/cm^3.

HOMO (highest occupied molecular orbital) values are determined by ultraviolet photoelectron spectroscopy,[38] and LUMOs (lowest unoccupied molecular orbital) are estimated from the optical gap of the material. Photoluminescence (PL) spectra are measured by a fluorescence spectrometer (EDINBURGH INSTRUMENTS) at the main absorption wavelength [296 nm for 4P-NPD, 367 nm for TCTA:$Ir(ppy)_3$]. Therefore, $Ir(ppy)_3$ is doped into TCTA to avoid concentration quenching.[39] For $Ir(ppy)_3$ the triplet energy is estimated from the peak emission wavelength. This method is further applied on the singlet energy of 4P-NPD and BPhen. The values for the triplet energy of 4P-NPD and BPhen, and the singlet energy level of $Ir(ppy)_3$, as well as the mobilities, are taken from literature.[25,37,40]

The photoluminescence spectra and the chemical structure of 4P-NPD and TCTA:$Ir(ppy)_3$ are shown in Fig. 1. The fluorescent blue emitter 4P-NPD has a main emission peak

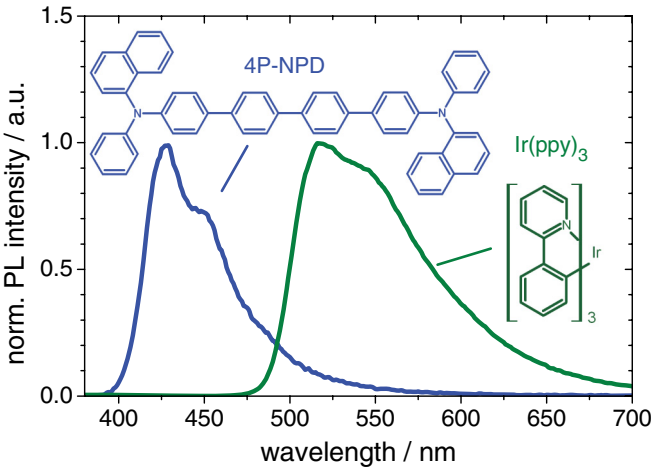

FIG. 1. (Color online) Chemical structure and normalized photoluminescence emission spectra of 4P-NPD (10 nm, bulk layer) and $Ir(ppy)_3$ [10 nm, doped in TCTA (10 wt%)].

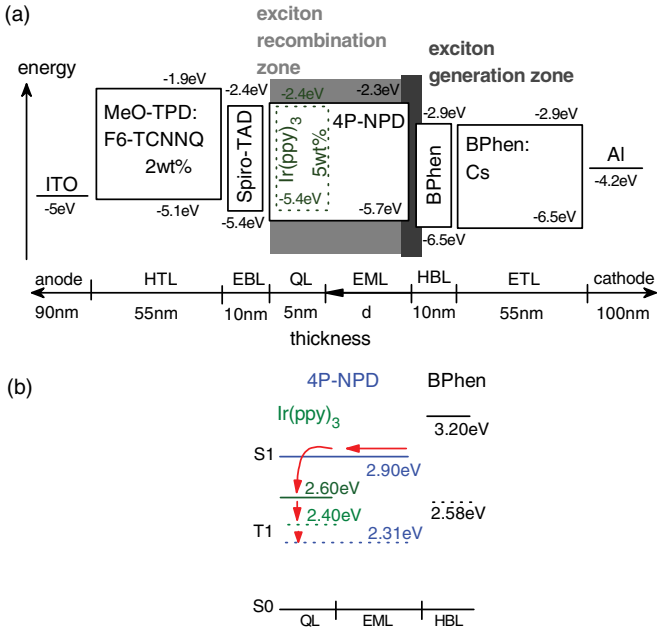

FIG. 2. (Color online) (a) Device architecture and energy level diagram of the blue fluorescent OLED. Due to the high hole mobility of 4P-NPD, the exciton generation zone (dark gray box) is assumed to be located at the 4P-NPD/BPhen interface. The singlets can diffuse in the direction of $Ir(ppy)_3$, and can recombine anywhere in the 4P-NPD layer (light gray box). (b) Singlets reaching $Ir(ppy)_3$ will be transferred to the singlet level of $Ir(ppy)_3$. The singlet exciton undergoes intersystem crossing to the triplet state of $Ir(ppy)_3$. Finally, the triplet is transferred to the 4P-NPD host and decays nonradiatively. As a result, the blue emission will be quenched compared to reference OLEDs without $Ir(ppy)_3$.

at 427 nm and a shoulder at 450 nm. The well known green phosphorescent emitter $Ir(ppy)_3$ exhibits the strongest emission peak at 517 nm. The resulting singlet and triplet energies are $S1(\text{4P-NPD}) = 2.90$ eV and $T1[Ir(ppy)_3] = 2.40$ eV.

C. Working principle of the device

A proposed energy level scheme of our device is depicted in Fig. 2(a). Charge carriers are injected via ITO and Al into the doped transport layers. Passing the thin blocking layers, the charges reach the EML. As 4P-NPD is a primarily hole transporting material (hole mobility $= 6.6 \times 10^{-4}$ cm^2/Vs, electron mobility $= 3.6 \times 10^{-8}$ cm^2/Vs), the exciton generation zone is assumed to be close to the HBL.[25,37] According to spin statistics, 25% singlets and 75% triplets are generated.[5] Both exciton species can diffuse before they recombine.

Since 4P-NPD is a fluorescent emitter, triplets will recombine nonradiatively. In contrast to the triplet harvesting concept,[4,37,41] the triplet energy of the quencher is chosen to be higher than that of the matrix material. Hence, triplets formed on 4P-NPD do not result in emission from the quencher. The singlets, on the other hand, have the possibility to recombine radiatively, nonradiatively, or to reach the quenching material. In the first case the generated photons might be coupled out and contribute to the emitted spectrum. A diffusion into the BPhen blocking layer is not possible, due to the 0.3 eV higher singlet level. Due to the high PL-efficiency (92%),[3] the probability for nonradiative decay can be neglected in 4P-NPD. As indicated in Fig. 2(b), singlets reaching the QL are transferred to the deeper lying singlet level of the $Ir(ppy)_3$ guest. Due to the strong spin orbit coupling,[42] the singlet exciton undergoes intersystem crossing to the triplet state of $Ir(ppy)_3$. Finally, the triplet is then transferred to the 4P-NPD host, where it undergoes a nonradiative decay. Therefore, we expect no contribution of $Ir(ppy)_3$ to the emitted spectrum. A thickness variation of the EML will lead to a different intensity of outcoupled emission from singlets, and the emitted spectra can be used to determine the singlet diffusion length.

III. THEORY

In this section we present an analytical model based on boundary conditions to calculate the singlet diffusion length in 4P-NPD using thickness dependent emission measurements of the operating OLEDs described above. For singlet excitons, the one-dimensional, steady state diffusion equation is given by[25,26]

$$D\frac{d^2n(x)}{dx^2} - \frac{n(x)}{\tau} + G_0 e^{-x/g} = 0. \tag{1}$$

The first term describes the diffusive transport, the second the monomolecular decay, and the third the generation of excitons along the diffusion direction x. Here, $n(x)$ is the singlet exciton density and D is the diffusion coefficient, which is assumed to be isotropic and constant in the whole 4P-NPD layer. The diffusion length L and D are connected via the exciton lifetime τ:

$$L = \sqrt{D\tau}. \tag{2}$$

As shown by Wünsche *et al.*,[25] it is very likely that the generation zone is not a delta-shaped peak at the interface where holes and electrons meet, but somewhat smeared out. The generation rate at $x = 0$ is given by G_0, and g is the distance from the interface when G_0 is decreased by a factor of $1/e$. Quenching/annihilation mechanisms including singlet-singlet annihilation, singlet-triplet annihilation, and singlet-polaron annihilation are neglected. We will show in Sec. IV C that these effects are only significant at very high current densities.

Furthermore, the singlet exciton current density $j_s(d)$ (or singlet flux) into the quenching layer is given by Fick's law:

$$j_s(d) = -D\frac{dn}{dx}. \tag{3}$$

The high singlet level of BPhen (3.20 eV) exhibits an efficient energy barrier for 4P-NPD singlets (2.90 eV) [cf. Fig. 2(b)]. Hence, it can be assumed that the singlet exciton current through BPhen is negligible, which results in the first boundary condition

$$\frac{dn(0)}{dx} = 0. \tag{4}$$

This implies that there is no concentration gradient for the exciton current, so excitons can still exist at the EML/HBL interface. The second boundary condition is obtained by the assumption of perfect quenching of singlets on the $Ir(ppy)_3$ molecule. At the interface to the quenching layer, the number of singlets is therefore

$$n(d) = 0. \tag{5}$$

However, singlet transfer to $Ir(ppy)_3$ can occur via both Förster and Dexter transfer, while the efficiency of each transfer is unknown. Using spectral overlap method,[43] the Förster radius can be estimated to be 2–3 nm for 4P-NPD:$Ir(ppy)_3$ and is in the same order of magnitude as the expected singlet diffusion length. Dexter transfer usually takes place over shorter distances. Neglecting an effective (combined Förster and Dexter) transfer radius from 4P-NPD to $Ir(ppy)_3$ leads, therefore, to an overestimation of the singlet diffusion length.[23,24]

Using the two boundary conditions, Eqs. (4) and (5), the solution of the steady state equation [Eq. (1)] reads[25]

$$n(x) = \frac{gG_0\tau}{L^2 - g^2}\left(2\frac{Le^{-d/L} + ge^{-d/g}}{e^{d/L} + e^{-d/L}}\cosh\frac{x}{L} - Le^{x/L} - ge^{-x/g}\right). \tag{6}$$

To derive the singlet diffusion length L, we have to connect the calculated singlet exciton current density $j_s(d)$ to the experimentally accessible radiance of the OLED devices. From the measured radiance $L_r(\lambda,0^\circ)$ in forward direction, the photon flux PF (number of outcoupled photons) is calculated using the assumption of Lambertian emission characteristics:

$$PF = \frac{\pi A_{\mathrm{OLED}}}{hc}\int_{380\,\mathrm{nm}}^{780\,\mathrm{nm}} \lambda L_r(\lambda,0^\circ)d\lambda, \tag{7}$$

where A_{OLED} is the active area of the device, λ denotes the wavelength, h the Planck constant, and c the speed of light in a vacuum. The Lambertian assumption is chosen to simplify the method. We provide angular dependent measurements in the supplemental material, showing that a Lambertian emission is an appropriate simplification.[44] The photon flux of the reference devices without $Ir(ppy)_3$ represents the number of all singlets. The photon flux of the devices containing $Ir(ppy)_3$ represents the number of singlets which do not reach the quenching layer. Hence, the singlet flux into the quenching layer for a certain EML thickness d is proportional to the difference:

$$j_s(d) \propto PF_{w/o\,Ir(ppy)_3}(d) - PF_{w\,Ir(ppy)_3}(d). \tag{8}$$

We note that at a constant current density, the number of injected charge carriers is constant for all devices. The PF is proportional to the external quantum efficiency[45,46]

$$EQE = \gamma \cdot q_{\mathrm{eff}} \cdot \eta_{\mathrm{out}}, \tag{9}$$

where γ is the so-called charge balance factor, describing the ratio of generated excitons to the number of injected electron-hole pairs. Since we use blocking and doped transport layers, we expect γ to be in the range of 70 to 90%.[31,32,45] The term q_{eff} is the effective internal quantum efficiency, which depends on the optical surrounding of the emitter. It describes the ratio of generated photons to the number of generated excitons.

The last factor η_{out} is the outcoupling efficiency, e.g., the ratio of outcoupled to generated photons. To overcome differences in outcoupling efficiencies, we use reference devices without the dopant $Ir(ppy)_3$. These devices consist of the same layer thicknesses to ensure that the position of the generation zone is kept at a constant position inside the device. In this case, q_{eff} and η_{out} can be considered as constant in the quenching and in the reference devices for one thickness d. A change in charge balance cannot be fully excluded, as $Ir(ppy)_3$ acts as a hole trapping molecule.[39,47] This will be considered later in the form of an additional term for direct recombination.

The final equation used to fit the data resulting from the spatial derivative of the exciton distribution in Eq. (6) reads[25]

$$j_s(d) = -A\left[\left(e^{\frac{d}{L}} + \frac{g}{L}e^{-\frac{d}{L}}\right)\tanh\frac{d}{L} - e^{\frac{d}{L}} + e^{-\frac{d}{g}}\right] + B. \tag{10}$$

The term A is a proportionality constant, including the first factor in Eq. (6), the diffusion coefficient, the effective internal quantum efficiency, and the outcoupling efficiency. Term B is motivated by direct recombination processes as shown in the work of Wünsche *et al.*,[25] who demonstrated a non-negligible electron current through these kinds of devices. Furthermore, term B compensates possible changes in charge balance.

IV. RESULTS

In a preliminary experiment we investigate the optimum thickness of the $Ir(ppy)_3$ doped quenching layer. Complete quenching of singlets at the QL/EML interface is required to ensure that the second boundary condition in our experiment is fulfilled. At the same time the influence of the quenching layers on the charge carrier balance has to be kept as small as possible. We vary the quenching layer thickness from 3 to 12 nm (cf. supplemental material for data and discussion).[44] For quenching layers thicker than 5 nm the external quantum efficiency is constant, meaning that no additional quenching processes are taking place. Furthermore, complete quenching of singlets at the $Irppy_3$ molecules is observed. Therefore, 5 nm is used as the quenching layer thickness. The influence of the QL on charge carrier balance will be discussed in the following section.

A. IV and spectral emission

To determine the singlet diffusion length, we vary the thickness d of the pure 4P-NPD layer between the exciton generation zone and the quenching layer. To overcome the influence of the optical cavity we design a reference device [without $Ir(ppy)_3$] for each thickness d (cf. Sec. II, Fig. 2). The IV characteristics of these devices are shown in Fig. 3.

The IV curves for one specific distance are in good agreement. For high current densities (>60 mA/cm^2) the voltage is slightly higher for the devices containing $Ir(ppy)_3$, which might be a result of hole injection and transport on the $Ir(ppy)_3$ molecules since Spiro-TAD and $Ir(ppy)_3$ have the same HOMO energy [cf. Fig. 2(a)], and $Ir(ppy)_3$ has hole trapping properties.[39,47]

Figure 4 shows the radiance in the forward direction for all 16 OLEDs when driven at a current density of 15.4 mA/cm^2. It can be nicely seen that the radiance decreases with decreasing thickness for the devices containing $Ir(ppy)_3$, which results from the quenching of singlets. On the other hand, the devices without $Ir(ppy)_3$ show a slight increase in emission intensity. This might be the result of a possible change in charge balance and/or an optical effect of the larger cavity. Since we can assume that the same effects are present in the devices with

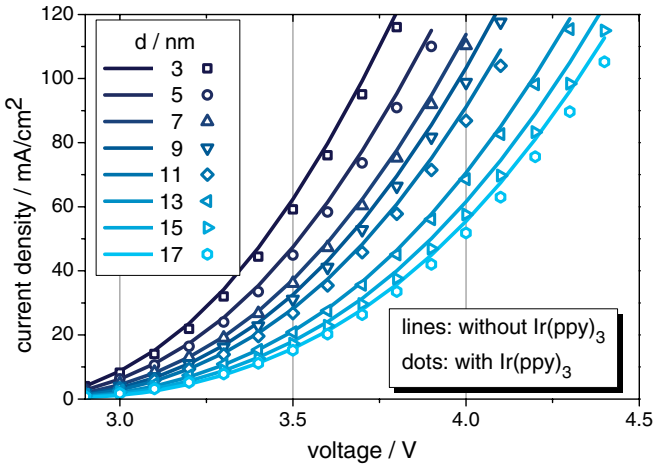

FIG. 3. (Color online) IV curves of the devices under investigation for different ETL thicknesses d. Reference devices [no $Ir(ppy)_3$] are presented by lines, and the devices with $Ir(ppy)_3$ are presented by dots. For one specific distance d, the IV curves of the devices with and without $Ir(ppy)_3$ are overlapping up to a current density of ca. 60 mA/cm^2, meaning that electrical effects of the dopant are not detectable. At higher current densities the devices with $Ir(ppy)_3$ require a slightly higher voltage.

$Ir(ppy)_3$ this is not a crucial issue. As discussed in Sec. II C emission from $Ir(ppy)_3$ is not observed in the measured spectra. This simplifies the presented method, as the photon flux can be directly quantified by the 4P-NPD emission spectrum without any corrections.

We expect the angular emission characteristics to be independent from the applied current, since the normalized emitted spectra in the forward direction are not changing significantly with applied current (see supplemental information).[44] Furthermore, the depicted devices show very similar angular dependent emission intensities at a current density of 15.4 mA/cm^2 (see supplemental information),[44]

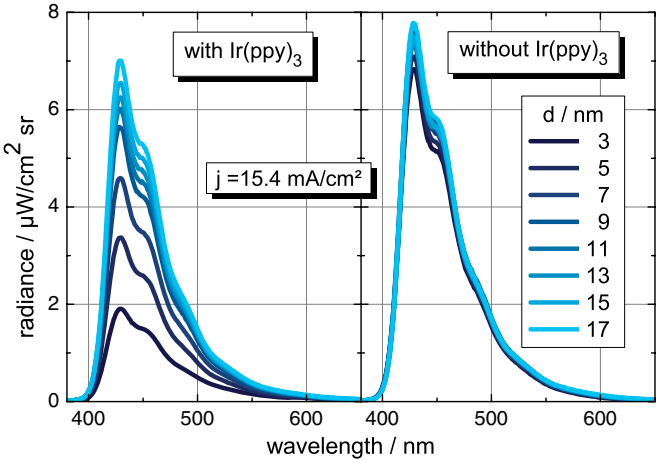

FIG. 4. (Color online) Measured radiance in the forward direction for different thicknesses d at a current density of 15.4 mA/cm^2. The increase in emission with EML thickness for devices containing $Ir(ppy)_3$ results from the lower number of quenched singlets. In contrast, the emission in devices without $Ir(ppy)_3$ is slightly enhanced. further substantiating the fact that optical effects are of minor importance.

B. Generation zone

Using Eq. (8) and the spectral radiance measurements, we calculate the photon flux and the exciton current of nonquenched singlets for different thicknesses in order to investigate the generation zone width. The generation zone is the region where holes and electrons meet and the exciton generation takes place. It has to be distinguished from the recombination zone and from the emission profile. The emission profile results from the emission of the excitons after possible Förster or Dexter transfers. The generation zone cannot be directly deduced from the emission profile.

Due to the high hole mobility of 4P-NPD, we expect the generation zone to be very narrow in comparison to the whole EML layer thickness and close to the 4P-NPD/BPhen interface. We investigate the photon flux at a current density of 15.4 mA/cm^2. As shown in Fig. 5, the photon flux decreases with increasing distance d from the exciton generation zone. In Sec. III we showed that the photon flux is directly proportional to the singlet exciton current inside the OLED. The decrease in PF confirms that the exciton generation takes place next to the HBL.

The lines are fits using Eq. (10). The width of the generation zone g is varied between 0.1 and 2 nm. It can be clearly seen that the peak of the fits is shifted to larger distances with increasing g. The three other fit parameters, the diffusion length L, A, and B, are adjusted to fit the experimental data. From $g = 0.1$ to 1 nm the parameters do not change significantly, and a good fit to the experimental data can be obtained. However, for $g = 1.5$ and 2 nm the diffusion length decreases (inset of Fig. 5) and the fits deviate more from the experimental data, especially for small distances from 3 to 7 nm. Therefore, it can be concluded that the generation

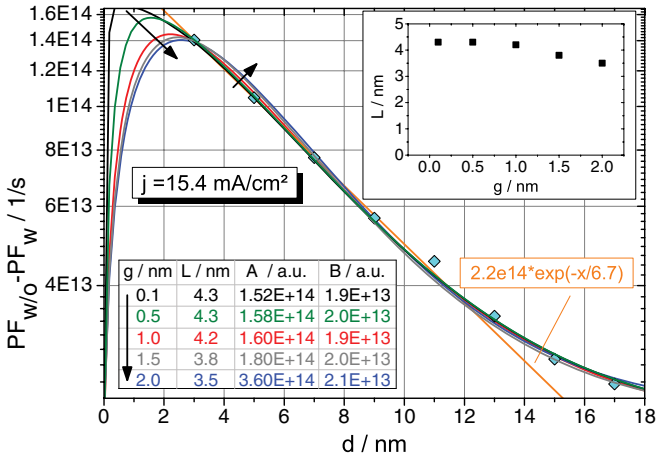

FIG. 5. (Color online) Photon flux depending on the distance d at a current density of 15.4 mA/cm^2 (dots). The fits (lines) according to Eq. (10) are describing different broadness g of the generation zone. The fit parameters are given in the table. A simple exponential decay (orange straight line) leads to an overestimation of the diffusion length. Inset: Dependence of the diffusion length L on the width of the generation zone g.

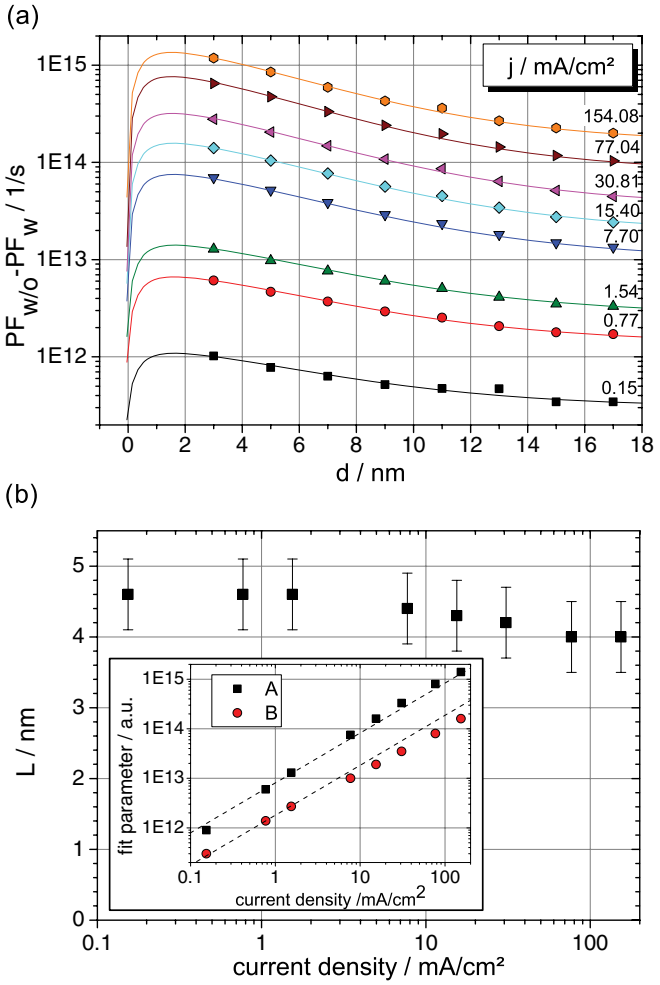

FIG. 6. (Color online) (a) Photon flux versus distance d for different current densities (symbols) and fitted emission profiles using Eq. (10) for different current densities (solid lines). A generation zone width of $g = 0.5$ nm is applied. (b) The extracted singlet diffusion length shows a slight dependency on the current density. The inset shows the obtained values for the parameters A and B. The dotted lines represent lines with a slope to the power of 1.

zone has to be smaller than 1.5 nm. In further calculations we will use $g = 0.5$ nm. This is lower than $g = 3$ nm obtained by Wünsche *et al.*,[25] but still in agreement with the fact that values from 0 to 7 nm lead to reasonable fits for the triplet diffusion length in 4P-NPD. As the generation of both singlets and triplets is the result of the gathering of holes and electrons, the generation zone width should not depend on the exciton species.

Using a monoexponential decay fit (orange straight line in Fig. 5) like in the work of Choukri *et al.*,[30] i.e., assuming a delta-shaped generation zone and no direct recombination processes, we obtain a value of 6.7 nm. The assumption of a too thin generation zone and the neglect of direct recombination leads to an overestimation of the singlet diffusion length.

A more detailed analysis of the width of the generation zone might be obtained from additional experimental data in the small distance regime ($d = 1$–3 nm). However, the closer the QL is to the generation zone the more singlets are quenched, and the detectable emission is dramatically lowered.

TABLE I. Fit parameter values from Fig. 6 for different applied current densities, according to Eq. (10). A describes the emission layer intensity and B the direct charge-carrier recombination. L is the singlet diffusion length. The width of the generation zone g is fixed to 0.5 nm for the calculated fits.

j (mA/cm^2)	0.15	0.77	1.54	7.70	15.40	30.81	77.04	154.08
L (nm)	4.6	4.6	4.6	4.4	4.3	4.2	4.0	4.0
$A \times 10^{13}$ (a.u.)	0.09	0.60	1.3	7.5	16	33	80	140
$B \times 10^{13}$ (a.u.)	0.03	0.14	0.27	1.3	1.9	3.5	8.0	16

C. Singlet diffusion length in 4P-NPD

The photon flux fitted by Eq. (10) is shown in Fig. 6(a) for different applied current densities. As motivated in Sec. IV B, we choose $g = 0.5$ nm as the width of the generation zone. The parameter A is adjusted to fit the height and B to fit the tail. A more detailed investigation of the fitting parameters and errors is given in the supplemental material. Regarding the accuracy of the fits, we estimate an error of ± 0.5 nm for the singlet diffusion length.

We obtain a good fit even at high current densities. The fitting parameters are summarized in Table I and plotted in Fig. 6(b). The diffusion length slightly decreases from 4.6 to 4.0 nm for increasing current density, i.e., the exciton density. In our model, the singlet diffusion length should be independent from the applied current. However, at a higher current density, several annihilation processes (singlet-triplet, singlet-polaron, singlet-singlet quenching) are present which lower the exciton current into the quenching layer and explain the decrease in singlet diffusion length. The small decrease with increasing excitation density indicates that secondary effects like annihilation processes, as well as change in charge balance and change in generation zone width, which we neglect in our model, play a minor role.

As shown in the inset of Fig. 6(b), the parameter A increases linearly with current density, while the parameter B (including effects of direct recombination and changes in charge balance) differs slightly for high current densities from the slope to the power of 1.

At a low current density of 0.15 mA/cm^2 we find a singlet diffusion length of 4.6 ± 0.5 nm, which is comparable to the value of 5.1 ± 1.0 nm obtained by Lunt *et al.*[23] using spectral-resolved photoluminescence measurements for N,N′-Di(naphthalen-1-yl)-N,N′-diphenyl-benzidine (NPD), a material with generally similar properties[3] that chemically differs from 4P-NPD only by two phenyl rings.

V. SUMMARY AND CONCLUSIONS

In summary, we present a simple and accurate method to measure the singlet diffusion length in 4P-NPD. Using a carefully chosen OLED structure with a narrow singlet generation zone and a suitable quenching material, we obtain the singlet diffusion length for a range of applied current densities. Boundary conditions like ideal blocking and quenching of singlets are discussed. An analytical model based on these

boundary conditions is presented. We have shown that the expansion of the generation zone, as well as the amount of direct recombination processes, are crucial parameters when calculating the diffusion length. By this means, we obtain a singlet diffusion length of $L = 4.6 \pm 0.5$ nm for a low current density of 0.15 mA/cm^2, where annihilation processes are insignificant. Furthermore, this method provides an estimate of the emission profile in our devices, which is otherwise hardly accessible in small-molecule OLEDs. Our method can be applied to other materials as long as the OLED structure ensures a narrow generation zone close to one of the blocking layers and an efficient quenching of excitons. Thus, the dependence of the singlet diffusion length on different material parameters, like crystal orientation, fluorescent yield, and others, can be investigated in the future.

ACKNOWLEDGMENTS

Novaled AG, Dresden is acknowledged for material support. The work leading to these results has received funding from the European Community's Seventh Framework Programme under Grant No. FP7–224122 (OLED100.eu).

*simone.hofmann@iapp.de
†Current address: Novaled AG, Tatzberg 49, 01307 Dresden, Germany.
‡leo@iapp.de.; http://www.iapp.de

[1] Z. B. Wang, M. G. Helander, J. Qiu, D. P. Puzzo, M. T. Greiner, Z. M. Hudson, S. Wang, Z. W. Liu, and Z. H. Lu, Nat. Photonics **5**, 753 (2011).
[2] S. Reineke, F. Lindner, G. Schwartz, N. Seidler, K. Walzer, B. Lüssem, and K. Leo, Nature (London) **459**, 234 (2009).
[3] G. Schwartz, M. Pfeiffer, S. Reineke, K. Walzer, and K. Leo, Adv. Mater. **19**, 3672 (2007).
[4] T. C. Rosenow, M. Furno, S. Reineke, S. Olthof, B. Lüssem, and K. Leo, J. Appl. Phys. **108**, 113113 (2010).
[5] M. A. Baldo, D. F. O'Brien, M. E. Thompson, and S. R. Forrest, Phys. Rev. B **60**, 14422 (1999).
[6] J. J. M. Halls, K. Pichler, R. H. Friend, S. C. Moratti, and A. B. Holmes, Appl. Phys. Lett. **68**, 3120 (1996).
[7] P. Avakian and R. E. Merrifield, Phys. Rev. Lett. **13**, 541 (1964).
[8] C. L. Braun, Phys. Rev. Lett. **21**, 215 (1968).
[9] S. D. Babenko, V. A. Benderskii, V. I. Goldanskii, A. G. Lavrushko, and V. P. Tychinskii, Phys. Status Solidi B **46**, 91 (1971).
[10] A. K. Ghosh and T. Feng, J. Appl. Phys. **49**, 5982 (1978).
[11] R. Signerski and G. Jarosz, Phot. Lett. Poland **3**, 107 (2011).
[12] D. Kurrle and J. Pflaum, Appl. Phys. Lett. **92**, 133306 (2008).
[13] S. Banerjee, A. P. Parhi, S. S. K. Iyer, and S. Kumar, Appl. Phys. Lett. **94**, 223303 (2009).
[14] N. Matsusue, S. Ikame, Y. Suzuki, and H. Naito, J. Appl. Phys. **97**, 123512 (2005).
[15] S. Cook, H. Liyuan, A. Furube, and R. Katoh, J. Phys. Chem. C **114**, 10962 (2010).
[16] D. E. Markov, E. Amsterdam, P. W. M. Blom, A. B. Sieval, and J. C. Hummelen, J. Phys. Chem. A **109**, 5266 (2005).
[17] S. Cook, A. Furube, R. Katoh, and L. Han, Chem. Phys. Lett. **478**, 33 (2009).
[18] A. J. Lewis, A. Ruseckas, O. P. M. Gaudin, G. R. Webster, P. L. Burn, and I. D. W. Samuel, Org. Electron. **7**, 452 (2006).
[19] H. Gommans, S. Schols, A. Kadashchuk, P. Heremans, and S. C. J. Meskers, J. Phys. Chem. C **113**, 2974 (2009).
[20] A. Holzhey, C. Uhrich, E. Brier, E. Reinhold, P. Bäuerle, K. Leo, and M. Hoffmann, J. Appl. Phys. **104**, 064510 (2008).
[21] J. Kalinowski, V. Fattori, and P. D. Marco, Chem. Phys. **266**, 85 (2001).
[22] R. Schüppel, T. Dienel, K. Leo, and M. Hoffmann, J. Lumin. **110**, 309 (2004).
[23] R. R. Lunt, N. C. Giebink, A. A. Belak, J. B. Benziger, and S. R. Forrest, J. Appl. Phys. **105**, 053711 (2009).
[24] S. R. Scully and M. D. McGehee, J. Appl. Phys. **100**, 034907 (2006).
[25] J. Wünsche, S. Reineke, B. Lussem, and K. Leo, Phys. Rev. B **81**, 245201 (2010).
[26] M. Lebental, H. Choukri, S. Chenais, S. Forget, A. Siove, B. Geffroy, and E. Tutis, Phys. Rev. B **79**, 165318 (2009).
[27] B. W. D'Andrade, M. E. Thompson, and S. R. Forrest, Adv. Mater. **2**, 147 (2002).
[28] Y. C. Zhou, L. L. Ma, J. Zhou, X. M. Ding, and X. Y. Hou, Phys. Rev. B **75**, 132202 (2007).
[29] C. W. Tang, S. VanSlyke, and C. H. Chen, J. Appl. Phys. **65**, 3610 (1989).
[30] H. Choukri, A. Fischer, S. Forget, S. Chénais, M.-C. Castex, D. Adès, A. Siove, and B. Geffroy, Appl. Phys. Lett. **89**, 183513 (2006).
[31] M. Furno, R. Meerheim, S. Hofmann, B. Lussem, and K. Leo, Phys. Rev. B **85**, 115205 (2012).
[32] S. Mladenovski, S. Hofmann, S. Reineke, L. Penninck, T. Verschueren, and K. Neyts, J. Appl. Phys. **109**, 083114 (2011).
[33] M. C. Gather, M. Flämmich, N. Danz, D. Michaelis, and K. Meerholz, Appl. Phys. Lett. **94**, 263301 (2009).
[34] S. L. M. van Mensfoort, M. Carvelli, M. Megens, D. Wehenkel, M. Bartyzel, H. Greiner, R. A. J. Janssen, and R. Coehoorn, Nat. Photonics **4**, 329 (2010).
[35] M. Pfeiffer, T. Fritz, J. Blochwitz, A. Nollau, B. Plönnigs, A. Beyer, and K. Leo, Adv. Solid State Phys. **39**, 77 (1999).
[36] J. Blochwitz, M. Pfeiffer, T. Fritz, and K. Leo, Appl. Phys. Lett. **73**, 729 (1998).
[37] G. Schwartz, S. Reineke, T. C. Rosenow, K. Walzer, and K. Leo, Adv. Funct. Mater. **19**, 1319 (2009).
[38] S. Olthof, W. Tress, R. Meerheim, B. Lüssem, and K. Leo, J. Appl. Phys. **106**, 103711 (2009).
[39] Y. Q. Zhang, G. Y. Zhong, and X. A. Cao, J. Appl. Phys. **108**, 083107 (2010).
[40] W. A. Luhman and R. J. Holmes, Appl. Phys. Lett. **94**, 153304 (2009).
[41] Y. Sun, N. C. Giebink, H. Kanno, B. Ma, M. E. Thompson, and S. R. Forrest, Nature (London) **440**, 908 (2006).
[42] M. A. Baldo, M. E. Thompson, and S. R. Forrest, Pure Appl. Chem. **71**, 2095 (1999).
[43] T. Förster, Ann. Phys. **6**, 55 (1948).

[44]See Supplemental Material at http://link.aps.org/supplemental/10.1103/PhysRevB.85.245209 for angular dependent emission intenstities, the discussion of the influence of the quenching layer thickness, the dependence of the spectral radiance on the applied current, and the estimation of the error of the singlet diffusion length.

[45]R. Meerheim, M. Furno, S. Hofmann, B. Lüssem, and K. Leo, Appl. Phys. Lett. **97**, 253305 (2010).

[46]C. Adachi, M. A. Baldo, M. E. Thompson, and S. R. Forrest, J. Appl. Phys. **90**, 5048 (2001).

[47]H.-H. Tsai, J.-H. Lee, and M.-K. Leung, Proc. SPIE **5937**, 593722 (2005).